[AMERICAN JOURNAL OF SCIENCE, VOL. 291, MAY, 1991, P. 473–506]

THE I/S-TO-ILLITE REACTION IN THE LATE STAGE DIAGENESIS

B. LANSON* and D. CHAMPION
Département de Géologie, Ecole Normale Supérieure,
24 rue Lhomond, 75231 PARIS Cedex 05, France

ABSTRACT. Decomposition of complex X-ray diffraction curves, image analysis of transmission electron micrographs, and X-ray fluorescence analyses of diagenetic clay fractions have been used to establish the co-existence of two mineral population types (I/S and illite) both of which evolve with depth in a well of the Paris Basin. This paper describes the I/S to illite transition. In this burial diagenesis setting, the proportion of I/S laths decreases greatly, but those that remain continue to grow. The proportion of illite hexagons increases, and the older grains appear to grow. The observed changes in crystal size distribution would be expected in a crystal growth process where one phase becomes unstable and is replaced by another.

XRF analyses of individual grains show that the I/S minerals become more illitic (near mica composition) with depth, but they always contain a portion of a smectite component, that is, silica-rich, low layer charge component. Both lath I/S and hexagonal illite minerals appear to grow by adding illite layers of the same composition (0.9 potassium atoms and a slight celadonite, phengite component) onto original crystallites.

This series of samples shows an I/S-illite phase change which is accomplished slowly in the rocks as they are subjected to burial diagenesis (time x temperature). Illite is the new phase; it is different from the I/S minerals.

INTRODUCTION

Mineralogical evolution of clay minerals was extensively described for over 20 yrs by many authors. Smectite illitization, especially, was shown in diagenetic series (Burst, 1969; Perry and Hower, 1970; Hower and others, 1976; Boles and Franks, 1979; Srodon, 1979 and 1984a; Velde, Suzuki, and Nicot, 1986; Glassman and others, 1989; among others) as well as in hydrothermal environments (Mac Dowell and Elders, 1980; Inoue and Utada, 1983; Horton, 1985; among others), in bentonites (Velde and Brusewitz, 1982), or in a contact metamorphism context (Nadeau and Reynolds, 1981). X-Ray diffraction (XRD) has been the essential tool used to reveal this evolution which is the mineral sequence

Smectite → random mixed-layer → ordered mixed-layer I/S → illite

When the lithology is homogeneous, there is a continuous decrease of smectite content of each of the illite/smectite interstratified minerals with increasing depth and thus with the pressure-temperature conditions. Comparing clay mineral evolutions in various wells of different

* Present address: U.S. Geological Survey, Box 25046, Mail Stop 404, Federal Center; Denver, Colorado 80225.

ages (Lahann, 1980; Srodon and Eberl, 1984; Velde, 1985; Velde, Suzuki, and Nicot, 1986; Jennings and Thompson, 1986; Freed and Peacor, 1989), it is obvious there is an important kinetic effect in this transformation. This is evident when the reaction progress of the maturation of organic material is compared to that of the clays in the same rock samples (Velde and Espitalié, 1989).

The precise reaction mechanism in diagenesis, although often speculated upon, has not been described in a series of diagenetically altered sediments. Many studies have proposed mechanisms (Hower and others, 1986; Boles and Franks, 1979), but the data have not been sufficiently complete to draw conclusions as to the nature of the reaction.

Information coming from various geological environments can be used by analogy in the determination of the characteristics of the diagenetic reaction:

Scanning electron microscope (SEM) allows one to observe the morphology of the crystals in the smectite to illite transition (Güven, Hower, and Davies, 1980; Pollastro, 1985; Keller, Reynolds, and Inoue, 1986; Inoue, 1986). Coming from hydrothermal, geothermal, and diagenetic environments all these materials have flaky particles when random I/S is dominant, lath-shaped particles associated with ordered I/S, and dominant hexagonal particles when the endmember illite becomes the essential phase.

Transmission electron microscope (TEM) studies confirm these SEM observations (Inoue, 1986; Inoue and others, 1987; Glasmann and others, 1989; Inoue and others, 1988) and permit one to quantify the morphological changes (Inoue and others, 1988). Using grain shape analysis, Inoue and others (1988) propose an Ostwald ripening process in natural I/S growth, as described by Baronnet 1974, 1982) for the growth of synthetic mica. Eberl and Srodon (1988) deduce such a process for the growth of illite using XRD diagrams and the Warren-Averbach technique (Warren and Averbach, 1950).

High resolution TEM lattice-fringe imaging also has been used to characterize the smectite to illite transition (Lee, Ahn, and Peacor, 1985; Ahn and Peacor, 1986), but interpretation of such images is very dependent on experimental conditions, especially focusing (Guthrie and Veblen, 1989). Thus it is difficult, with this technique, to determine if expandability is related to "real" mixed-layering effect or if it only results from interparticle diffraction (Ahn and Peacor, 1989). This technique is not reliable enough to determine if one of these two different ways to consider expandability is wrong.

In summary, XRD, SEM, and TEM have shown that the smectite to illite transition is a stepwise process involving three distinct crystal morphologies (flake, lath, and hexagon) and two crystallographic ordering behaviors (random and ordered). Comparison of different burial diagenesis sequences leads to the conclusion that the transformation is not only dependent on temperature but also time. Changes in the sizes of the crystallites suggest that a growth mechanism is involved in the

change. However, the growth mechanism and the composition of the crystallites are not known with precision. In fact there is, at present, debate over the composition of the individual particles. Nadeau and others (1984a, 1985) suggest that the I/S minerals are strictly of illite composition where the expanding layer is found at the surface of the crystallites giving an interparticle diffraction effect. The surface would be potassium-poor and would expand in contact with other particles sedimented on them in the sample preparation process. This is in contrast to the more classical assumption that the I/S minerals are epitaxially interlayered mixtures of illite and smectite layers. At present, there is no direct and reliable (see above the focusing problems on HRTEM) way to determine the origin of the expandability observed in the clay samples and thus the mechanism involved in this diagenetic process.

Another problem arises in that most of these studies were done on hydrothermally deposited material. There is no reason to assume that the same reaction mechanism will occur in precipitated materials and those due to recrystallization processes such as those encountered in diagenesis. We believe that the hydrothermal deposition and bentonite metasomatism (Velde and Brusewitz, 1982) reaction mechanisms should not be directly applied to diagenetic evolution of sediments.

Hydrothermal vein occurrences of illite/smectite minerals are not sequential, that is, they do not demonstrate a destabilization of one mineral to form another mineral by continuous reaction through the influence of increased temperature as is the case of diagenesis. They result from the precipitation of a series of minerals stable in increasing P,T,X conditions, but they do not imply a transformation of these minerals. Thus their use as models for diagenetic transformation is limited. Further, bentonite and hydrothermal illite/smectite (I/S) mineral chemical compositions are not the same as those found in diagenesis (Velde and Brusewitz, 1986; Meunier and Velde, 1980), and the reactions among them are therefore likely to be different from those found in pelitic, diagenetically altered rocks.

In the present study we investigate the end of the diagenetic smectite to illite transformation, the ordered I/S to illite reaction. The present study concentrates only on the diagenesis of clays in pelitic arenaceous rocks. We have studied cutting samples from a drill hole in the eastern part of the Paris Basin. XRD was used to characterize the mineralogical evolution along the series as precisely as possible; morphological changes were determined by TEM observations; and chemical data were collected with X-ray fluorescence micro-analyses on individual clay particles.

These sediments and pyroclastic rocks show the typical evolution of I/S minerals in the latter stages of diagenetic transformation. Pyroclastic and sandstone facies are especially useful because the I/S and illite crystallites have been able to develop fully, forming well defined crystallographic grain edges and shapes. This allows one to distinguish the

diagenetic from the detrital material and to observe the growth facies (shapes and relative abundances) of the grains.

The aims of the study are twofold: (1) to observe the transition between mixed layer mineral (I/S) and illite and thus the type of mineral reaction or mineral growth responsible for the changes seen in the X-ray diffraction diagrams of diagenetic clay minerals in deeply buried rocks, and (2) to characterize the phase illite.

X-ray diffraction (XRD) and electron microscope analysis are not new, but the treatment of the data obtained is new (decomposition of calculated and experimental XRD curves, quantification of grain populations obtained by electron microscope photographs, X-ray fluorescence chemical analysis of individual clay particles).

EXPERIMENTAL

Samples.—The samples were drill cuttings from a 2150 m deep bore hole in the eastern Paris Basin near the town of Nancy (supplied by the Institut Français du Pétrole). The top of the section is composed of 150 m of Dogger limestone followed by 220 m of argillaceous Liassic sediments and by 630 m of clay, evaporitic and sandy Triassic sediments, 340 m of volcano-detritic Permian sediments, and 800 m of detrital, sandy Stephanian red sediments. Sixty-two samples from the drill hole were used to establish the general diagenetic trend in the I/S minerals. Four of these which showed clearly the I/S transition stages were investigated in detail (morphological and chemical analysis on TEM). The essential criterion for the selection of these samples (from 1000, 1550, 1730, 2130 m depth) was the absence, or the very low abundance, of other phases such as chlorite, kaolinite, or carbonates to avoid confusion for TEM observations. The sample from 1000 m is from the volcano-detritic level. The different origins of the sediments could have an influence on their diagenetic evolution. The great consistency of the observations (see below) indicates that this influence was only minor, if it exists.

Several samples were chosen, due to availability and proximity to the overall I/S smectite content, to test the experimental method and to test the validity of the description of one sample as a representative of the stage of diagenetic alteration. Eleven samples from the same Jurassic outcrop near Lons le Saunier, in the French Jura were used to test the variability on the scale of a meter size outcrop. Five different stratigraphic levels (from Barremian to Kimmeridgian) were sampled in seven neighboring deep wells located in the Germigny/Coulomb area, East-Center of Paris Basin. These core samples were furnished by the Institut Français du Pétrole and Gaż de France to test the variability between samples coming from different but neighboring deep bore holes.

Experimental methods.—X-ray diffraction (XRD) of all samples was carried out on untreated, oriented, less than 2 μm fractions on glass slides using a Philips PW 2213/20 diffractometer with a stepping motor drive on the goniometer. Ni-filtered CuKα(1 + 2) radiation was used.

Motor and intensity acquisition commands were effected using a Socabim DACO system. Usual counting times and step size were respectively 3 sec and 0.01 °2Theta. If necessary greater counting times were used to obtain a better spectrum.

Usually, no exchangeable cation was used. But for some typical samples, patterns of Sr-saturated and untreated samples were compared, and no differences were found (Lanson and Besson, in preparation).

Decomposition method.—Typical air dried diffractograms from this series are shown in figure 1,and one can observe the classic decrease in smectite content from both the shift of peak position and the decrease of peak breadth.

Diffraction data were treated using decomposition methods outlined by Lanson and Besson (in preparation). Briefly they are as follows:

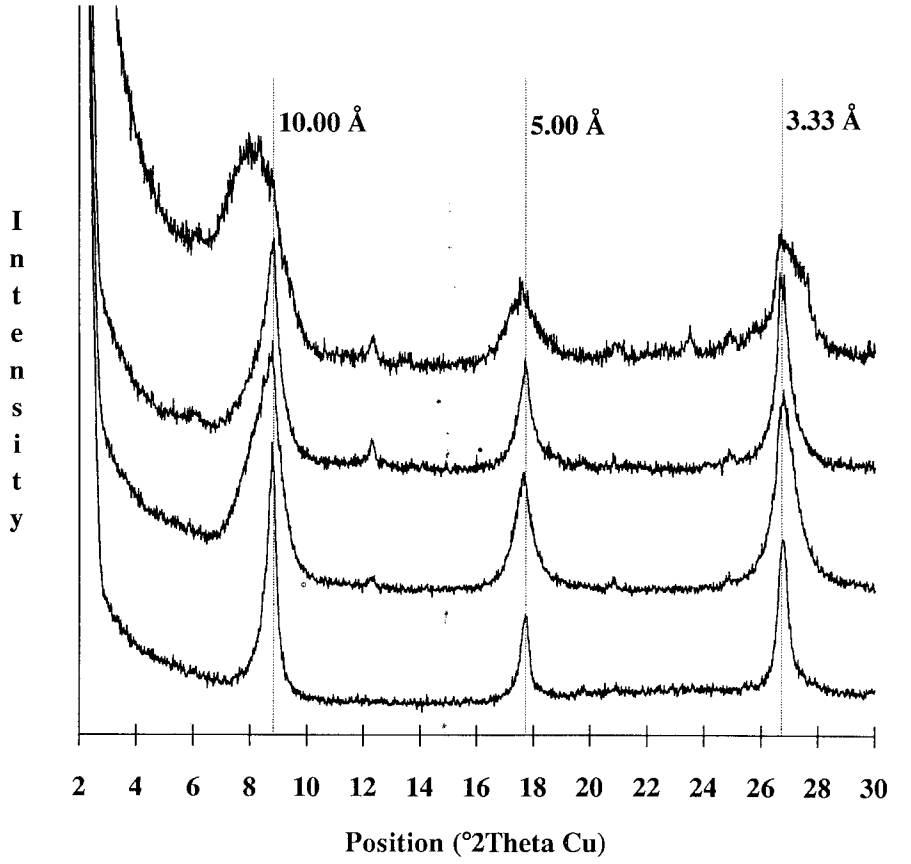

Fig. 1. XRD diagrams of air-dried clay preparations from the deep well studied (Paris Basin, France).

Only the near 10 Å band was considered due to its great intensity and to fewer problems of interference of other phases (chlorite and quartz) with higher order I/S reflections. Also, the effect of coherent scattering domain size on band width and position is greatest here, which gives additional information concerning the evolution of the clay particles in diagenesis.

The experimental diffraction traces were smoothed to remove the major statistical counting errors; smoothing was performed with a cubic spline fit on a nine point window (Lanson, ms; Lanson and Besson, in preparation). Background-stripping was performed on the smoothed raw diffraction curves; the procedure used was developed for this work and is described by Lanson (ms) and Lanson and Besson (in preparation).

A least squares iteration procedure or a downhill simplex iteration procedure (Nelder and Mead, 1965) was used to determine the best fit for the proposed bands of the complex experimental diffraction spectra. An intensity maximum was treated as a combination of Kα1 and Kα2 wavelengths due to the incomplete filtering of the CuKα radiation used. These double peaks were fitted using either Lorentzian or Gaussian distribution formulae until a best fit was found. Generally the Gaussian form appeared to give the closest approximation to the experimental curves.

If we exclude the chlorite peak, three elementary peaks were required for a good fit (fig. 2) to the complex XRD band between 4 and 10 °2θ Cu Kα (air dried patterns). Each of these peaks should be related with a distinct "phase"[1] to justify the decomposition treatment (Lanson and Besson, in preparation). A clay "phase" is not associated with an unique homogeneous material but represents a population of particles whose physico-chemical characteristics (smectite content, N values, nature, number, and position of the atoms in the structure) vary. Each of the "phases" identified with this decomposition method will be characterized by its mean value for each of these parameters. Thus these three XRD peaks should be related to the TEM observations to confirm the results obtained by XRD. Indeed it has been possible, with the TEM, to distinguish two I/S populations, plus the presence of detrital mica particles.

The glycolated patterns were fitted with three of four elementary peaks, depending on the expansibility of the most expandable I/S "phase." Theoretically, with three "phases" characterized on AD patterns, there should always be four peaks: one for detrital mica, one for the less expandable I/S (which is very close to illite composition), and two for the most expandable I/S (one on each side of 10.0 Å). These can be observed on figure 3A. But with increasing percent illite in this "phase," the

[1] The word "phase" is used with quotes, because it describes a population of particles whose physico-chemical characteristics vary about a mean value. It is assumed that this population behaves as a monophasic (in thermodynamic sense) material having the same mean characteristics. Consequently, the word phase (without quotes) is used in the thermodynamic sense throughout the rest of the paper for this mean material.

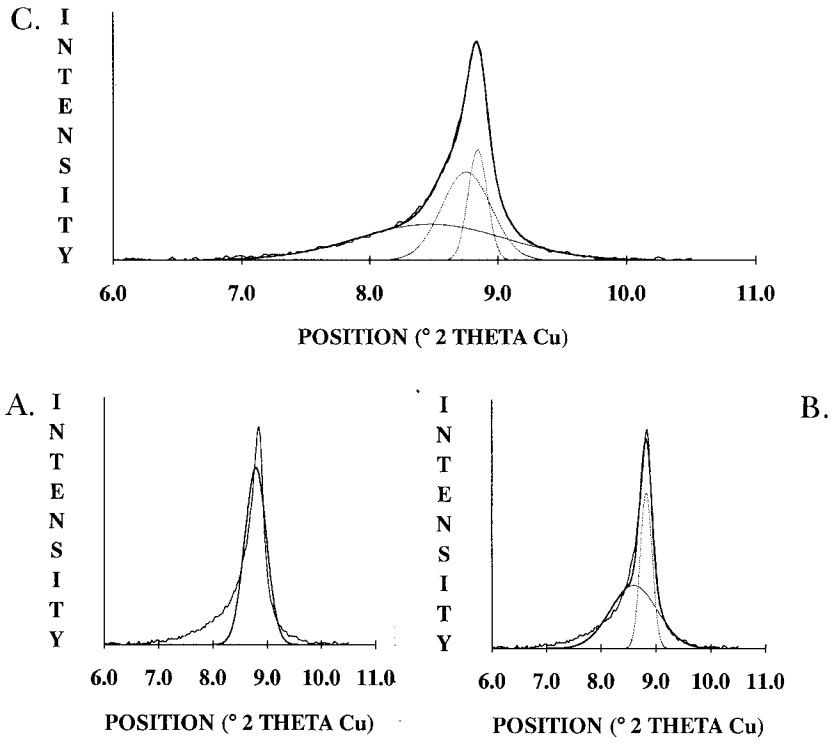

Fig. 2. Air-dried pattern of CHV2130 sample after Sr-exchange. Examples of decomposition with one (A), two (B), and three (C) elementary peaks. The best fit with three bands is obvious.

resolution of the method becomes insufficient to separate the peak of the I/S "phase" in the 10.0 Å zone from the illite peak (Lanson and Besson, in preparation). Therefore, in the deepest samples the decomposition of EG patterns was done with only three elementary peaks (see fig. 3B).

Reproducibility of the experimental method.—Reproducibility of the determination of elementary peak characteristics (position and width), and thus the applicability of the method to diagenesis study, was tested in the following manner:

1. A given sample was run at different scan speeds to test the importance of the initial data signal to background factor. Counting time has a weak influence on diffraction profiles, except that 1s counting time was unable to provide good counting statistics (Lanson, ms). There is no systematic variation of elementary peak characteristics (position and width) with increasing counting time. Thus, we can consider that patterns obtained with usual counting time (3 sec) are representative of the sample.

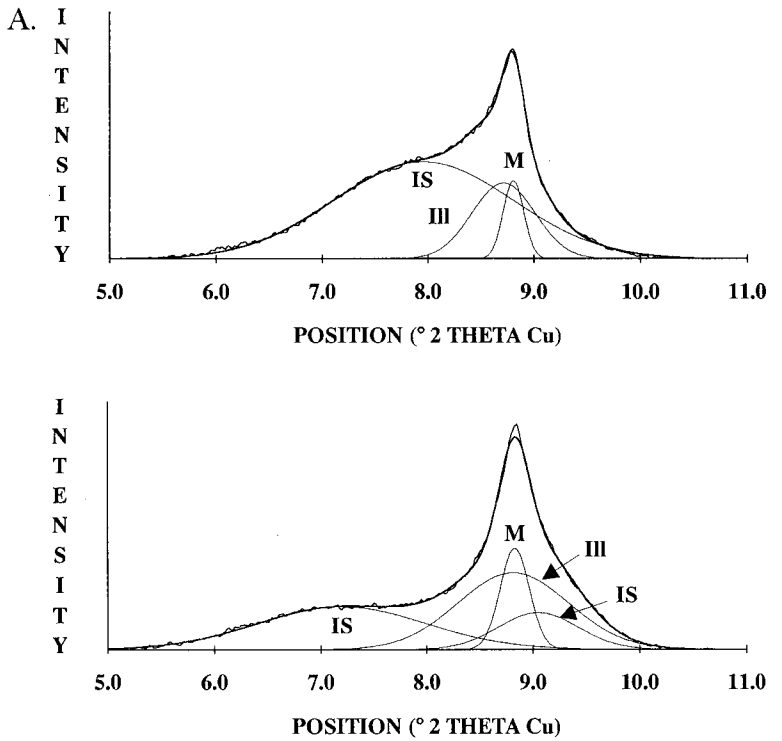

Fig. 3(A) Decomposition, after Sr-exchange, of air-dried (top) and glycolated (bottom) patterns of CHV1475. Peaks are labeled IS for the band representing the particle population with the higher expandability, Ill for the less expandable population (illite), and M for the micaceous, most likely detrital component.

2. A single slide sample was run 5 times to test for variations due to machine effects (statistical fluctuations in counting). The bands present at lower angles, with greater widths, show the greatest variations (Lanson, ms). These represent the material with the greatest expandabilities (smectite content in the mixed-layer I/S minerals) and the smallest average coherent domain size.

3. Five preparations of the same sample were made to test reproducibility of sample preparation techniques and influence of sample placement in the diffractometer. The standard deviations are similar to those obtained during tests for machine reliability, and thus we cannot distinguish between these two effects (Lanson, ms).

4. In order to assess the reliability of an estimation of diagenetic reaction progress (smectite to illite transformation) based on the study of one bore hole, several groups of samples were investigated. Eleven samples were taken from the same outcrop (Jurassic, found near Lons le Saunier in the French Jura). Five stratigraphic levels were sampled in

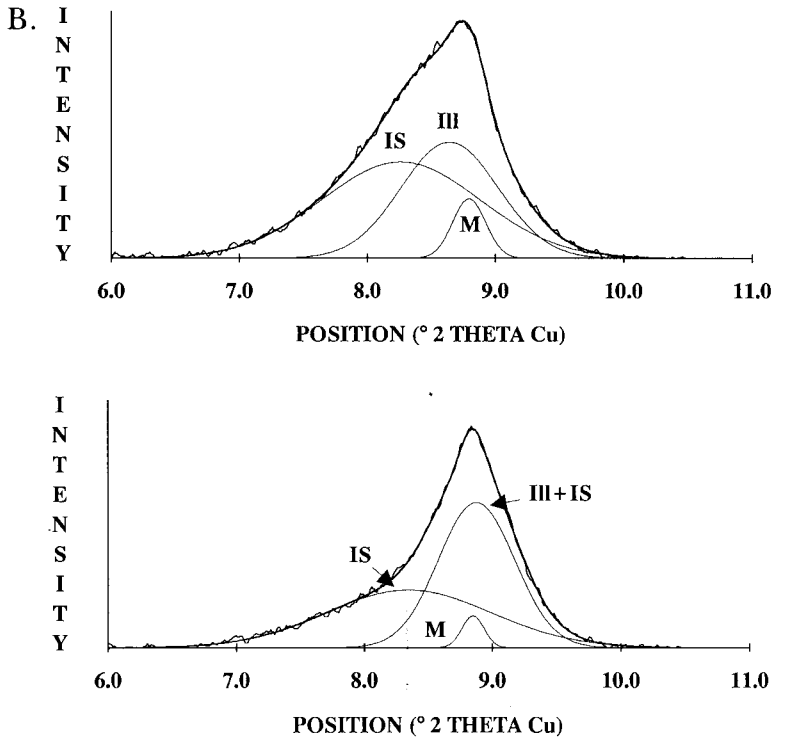

(B) Decomposition, after Sr-exchange, of air-dried (top) and glycolated (bottom) patterns of CHV1945.

seven wells in the East-Center of the Paris Basin (Germigny/Coulomb area). These tests for homogeneity in the same outcrop and in the same stratigraphic level in several neighbor wells demonstrate that the materials deposited in the same sedimentary facies show the same stage of reaction almost within the error of the determination method (Lanson, ms). Given the same sedimentary facies, diagenetic change of the clay is the same at given temperature and time conditions.

In conclusion, we can say that the decomposition method is a reliable tool for the characterization and identification of different phases contributions in complex XRD spectra of natural samples (Lanson, ms; Lanson and Besson, in preparation).

Simulated XRD diagrams.—The same decomposition methods (background stripping, Gaussian peak shape however without the Kα2 contribution) were used to measure the band positions and widths of peak generated using the Reynolds NEWMOD program (Reynolds, 1985) or a similar program written by G. Besson, University of Orléans. In the programs used to generate the X-ray diffraction spectra, the important variable parameters are the number of coherently diffracting layers, the

proportion of smectite and illite, and the degree of order in the I/S stacking. Particle orientation is also an important variable parameter (Reynolds, 1986); this parameter influences mainly absolute and relative intensities, but its effect on peak position and width seems to be weaker so that it was not considered in this study.

R = 1, with a maximum possible degree of order (no SS sequences possible if percent S < 50), was used to simulate these samples because diffractograms of the natural I/S minerals presented the major characteristics of this ordering type. Longer-range ordering units (R = 2, R = 3, R = n) were not used for illitic material containing less than 15 percent of expandable layers. For such I/S minerals the diffraction pattern is influenced mostly by the illite component. The ordering range has a weaker influence for such highly illitic materials. The patterns obtained for such illitic materials with long range ordering are quite similar to those obtained with short range, R = 1; at least, they show a similar trend either in peak position-percent smectite plot (see, for example, figs. 5 to 8 in Srodon, 1980; fig. 7 in Srodon, 1984b) or in a $\Delta 2\theta_1$-$\Delta 2\theta_2$ diagram (fig. 5 in Watanabe, 1988).

An example of the decomposition of a modelled diffraction pattern is given in figure 4. In the case of the modelled diffraction pattern, only the major band was considered. The subsidiary bands, related to the interference function oscillations (Reynolds, 1980 and 1989) and not to a distinct phase, were ignored. The expandability and the number of coherently diffracting layers in the csinβ direction (N in the Reynolds program) were estimated by comparing experimental peak position and half height width to those deduced from calculated patterns.

Image analysis.—The study of the grain morphology by transmission electron microscopy (TEM) follows the initial principles outlined by Inoue and others (1988) who studied a series of clays from hydrothermal vein deposits.

Samples selected for the present study contained very little chlorite and kaolinite. However the rare, very highly absorbing, large hexagonal flakes observed occasionally were avoided in the analysis. Irregular, thick grains were also avoided as they most likely represent detrital material identified in the XRD traces. Only grains presenting several sharply defined growth faces were analyzed; these represent more than half those on the photographs. Thus the grain morphologies noted are not taken to represent the totality of the grains subjected to X-ray diffraction analysis but the growing, diagenetic I/S minerals present in the sample. The selection made can bias the interpretation of absolute grain abundances. However, given that the selection was made on morphological grounds, we can say that the analysis that follows represents the grains that have well developed shapes.

Photographs were made of highly diluted samples which were ultrasonically dispersed and subsequently deposited on carbon coated copper grids. Observations were made using a Philips EM400 TEM system with an accelerating voltage of 80 kV. Figure 5 gives examples of

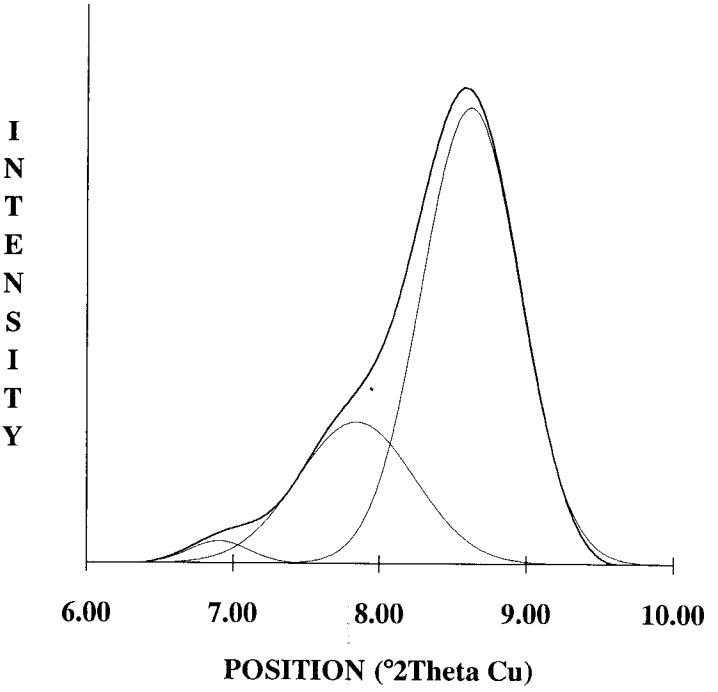

Fig. 4. Measurement, with the decomposition software, of position and half-height width for a simulated pattern. Only values of the greater angles peak are used to characterize this pattern; other peaks are due to interference oscillations (see text). Simulation conditions were illite 92 percent, smectite (2 interlayered water layers) 8 percent, R = 1 unit structure, coherent scattering domain sizes from 11 to 14 layers, with a continuous distribution.

the initial photographs used in the image analysis procedure. With several photographs of each sample, several hundred grain contours were traced on paper. These shapes were then digitized using a Benson system.

The resulting grain shapes were analyzed using the following procedure (fig. 6): an ellipse was inscribed in each particle convex outline. The axes of the ellipse were used to estimate the aspect ratio of the grains, that is, length to width. In using this method, the regular forms of the hexagon and equilateral triangle give an aspect ratio of one. Other methods, used for example by Inoue and others (1988), give different values of the greatest and smallest dimensions of the regular form and hence an aspect ratio greater than one.

A second parameter quantified is the equivalent circle diameter. This value is determined as the diameter of the circle that represents the surface area of the particle. This surface was computed by dividing the particle surface area using regular polygons and summing up their areas.

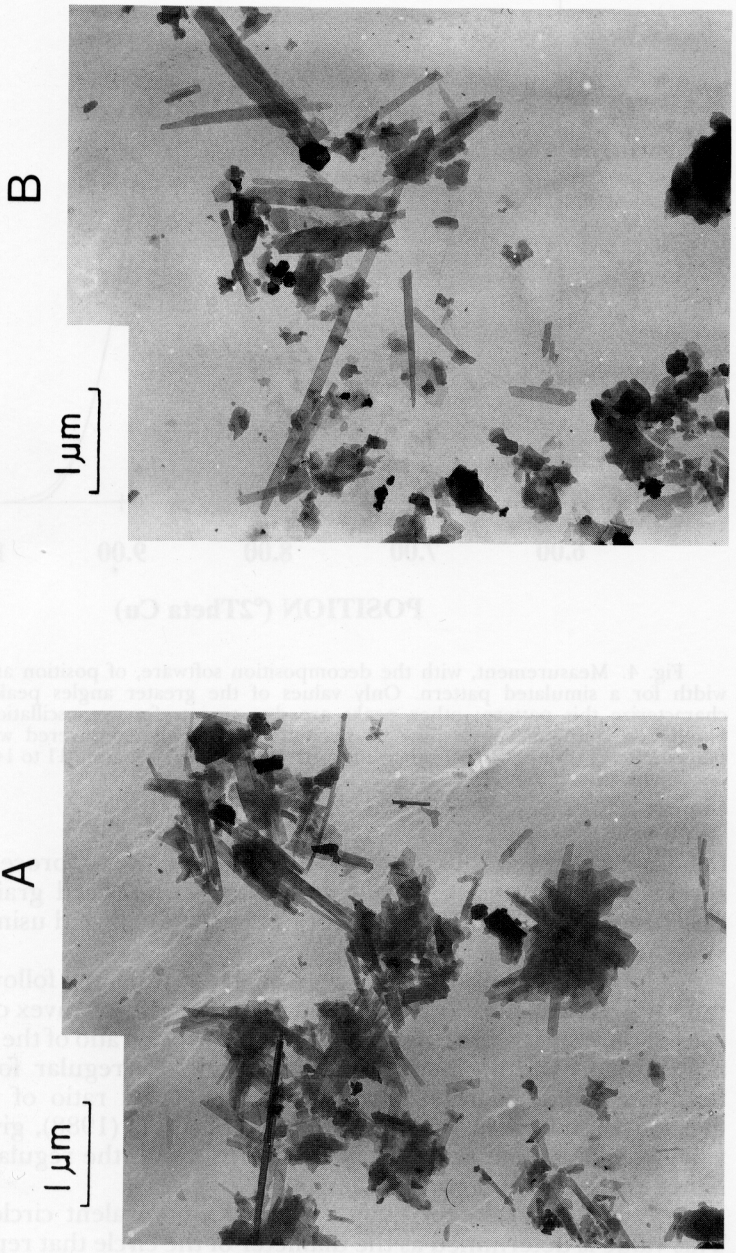
B
1 µm
A
1 µm

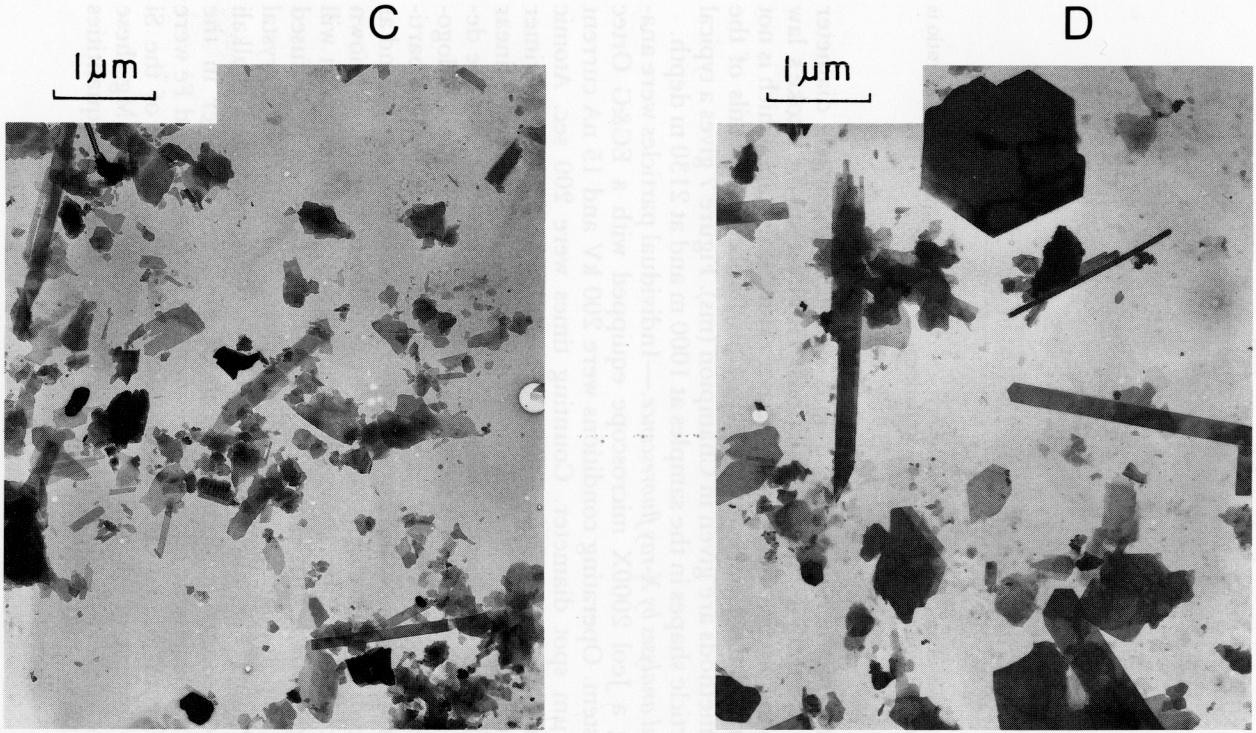

Fig. 5. TEM photographs of samples CHV1000 (A), CHV1550 (B), CHV1730 (C), AND CHV2130 (D) showing both lath- and hexagonal-shaped particles.

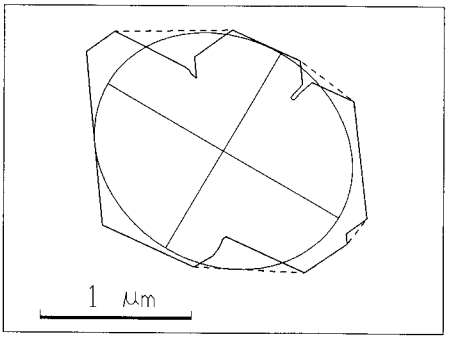

Fig. 6. Example of an ellipse inscribed in a typical clay mineral grain. The axes ratio is used to sort the grains into different shape populations.

The diameter of the equivalent circle is similar to a particle diameter assumed in the Stoke's Law calculations. However in the Stoke's law calculations the particle is assumed to have a spherical shape which is not the case for the flake particles typical of phyllosilicates. Details of the calculation methods are given in Champion (ms). Figure 7 gives a typical series of particle shapes in the samples at 1000 m and at 2130 m depth.

Chemical analyses by X-ray fluorescence.—Individual particles were analyzed using a Jeol 2000X microscope equipped with a EG&G Ortec detector system. Operating conditions were 200 kV and 15 nA current and a 0.5 µm spot diameter. Counting times were 200 sec. Atomic concentrations were estimated using the methods of Cliff and Lorimer (1975) for thin samples. Net intensities were determined from linear background-corrected spectra. K-factor correction coefficients were determined using synthetic muscovite, natural pyrophyllite, and phlogopite samples. These values for the standards were determined on particles giving approximately the same number of total counts per second as those of the diagenetic clay particles. The standards and the unknown samples should then have about the same particle thickness which will give homogeneous results especially from alkalis which can be diffused away from the point of beam impact due to charge build up in the crystal (Van der Pluijm, Lee, and Peacor, 1988). It is assumed that if alkali diffusion does occur, it does so in about the same manner in the standards and diagenetic clays. The elements Si, Mg, Al, K, and Fe were analyzed. Errors due to counting statistics were 2 percent of the Si present, 3 percent of Al, and 4 percent of K. For Fe and Mg these counting statistics errors can reach 15 percent, due to their low quantities in the samples studied.

EXPERIMENTAL RESULTS

X-ray diffraction.—A study of 62 samples for the well investigated at all depths showed that there were three elementary peaks (± chlorite

peak) present upon decomposition in most of the samples; they can be attributed to a mica, probably detrital, an I/S population with very few expanding layers present, and another I/S population which contains a greater, more variable number of expanding layers. In going down the bore hole to older rocks which have experienced higher temperatures, the micaceous and the illitic population change little in their characteristics (fig. 8). Peak position and width are rather constant. In the population with greatest expandability, the peak positions and widths both change indicating that there is a decrease in the apparent smectite content and/or increase of the mean coherent domain size (designated as N in the Reynolds program) in this population of particles. Change in smectite (expandable layer) content with depth is a typical diagenetic trend observed in many sequences previously studied (see Velde, 1985 for a summary), and it is the basis for the assumption of the smectite-to-illite conversion.

The four samples chosen from the well represent characteristic stages in the mineralogical change near the I/S to illite transition. According to the shift of peak position and to the decrease of half-height width, we can say that the smectite content of the most expandable I/S phase decreases with depth, and the coherent domain size increases. The elementary peaks fitted on experimental patterns are wider, for a given position, than those fitted on calculated patterns. This effect of peak broadening, has been known for a long time (Reynolds and Hower, 1970) but still remains unexplained (Reynolds, 1989). Therefore, the method allows an analysis of trends, but it is not possible, at present, to quantify either the decrease in smectite content and/or increase in coherent domain size. We have not yet experimented with either the thermal vibration of the atoms in the structure or the addition of stacking faults in the modeled stacking sequences, both of which can result in an appreciable peak broadening.

The slight decrease of peak width for the illitic phase indicates either a small increase of illite content, already very close to 100 percent, or an increasing coherent domain size (or both).

Image analysis.—Figure 9 shows the evolution of the size (equivalent diameter) distribution of all particles as a function of depth in the profile for the four samples analyzed. The general change noted is a widening of the histogram due to a relative increase in the proportion of larger grains with depth. There remains nevertheless a significant proportion of grains in the small size categories. These data strongly suggest that the clay particles that are older and have experienced higher temperatures increase their size through crystal growth.

In figure 10 which shows the abundances of the grains as a function of the log of the aspect ratio (L/W), it is apparent, at least at 1000 and 1550 m, that there are two main grain shape populations. In the photographs (fig. 5) and diagrams of grain shapes (fig. 7), these laths and more regular shapes based upon a hexagonal form can be identified at all depths. The more blunt shapes often have interface angles of 120° which

Figure 7

suggest hexagonal forms. Often these shapes are more rectangular in overall form than they are hexagonal. It should be noted that the short edges of the laths are often terminated by small edges, also forming an angle of 120°.

The range of aspect ratios log (length/width) does not change greatly with depth. At 1000 m, in the log representation (fig. 10), two modes are evident: one with a maximum at 0.15 and another near 0.6 (L/W of 1.4

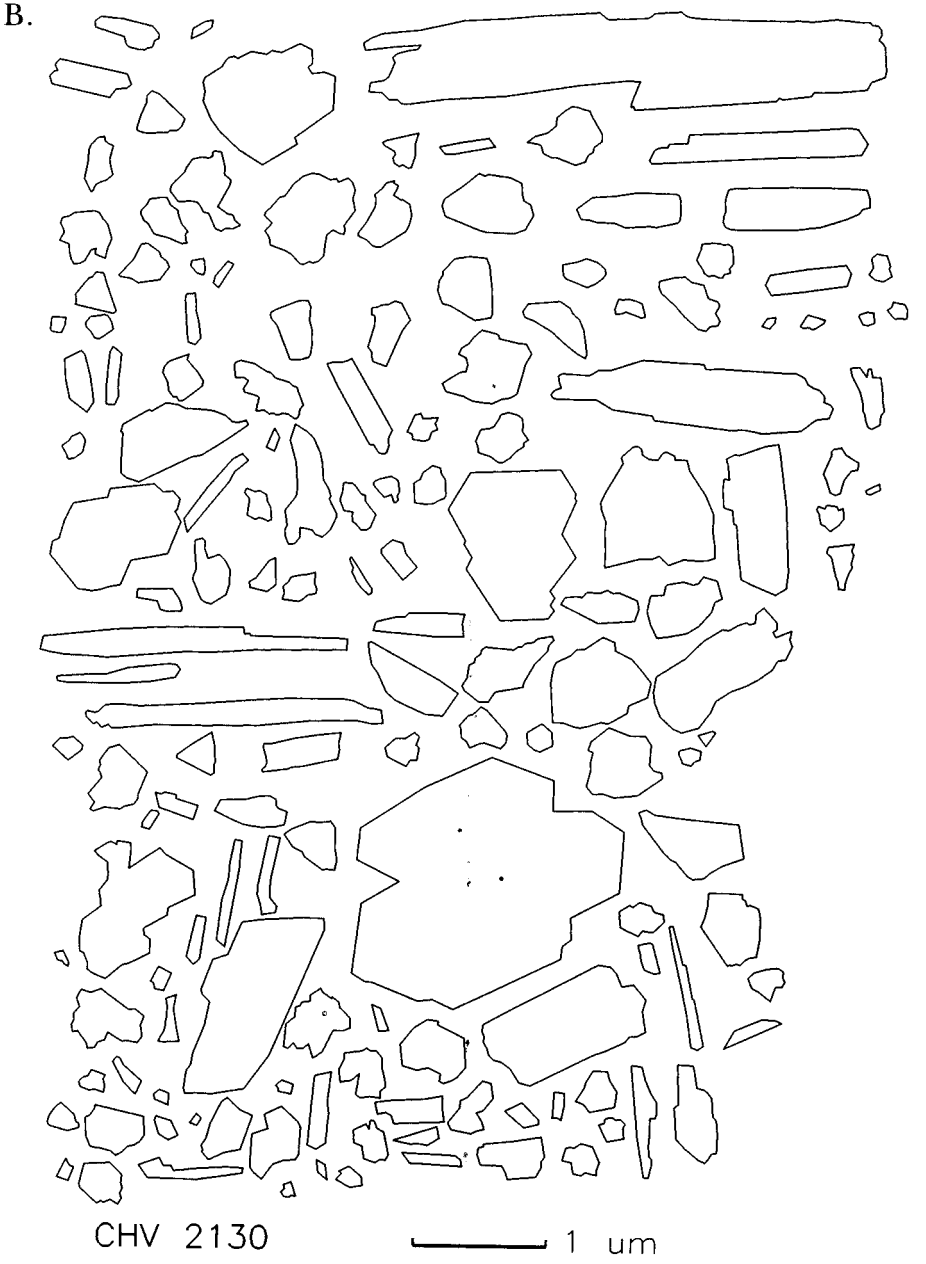

Fig. 7. Typical grain shapes in two of the samples studied, CHV1000 (A) and CHV2130 (B). Note the two dominant shape types, laths and hexagon-derived, which change in relative abundance and size as depth and diagenesis increase. A: ×22,500; B: ×17,500.

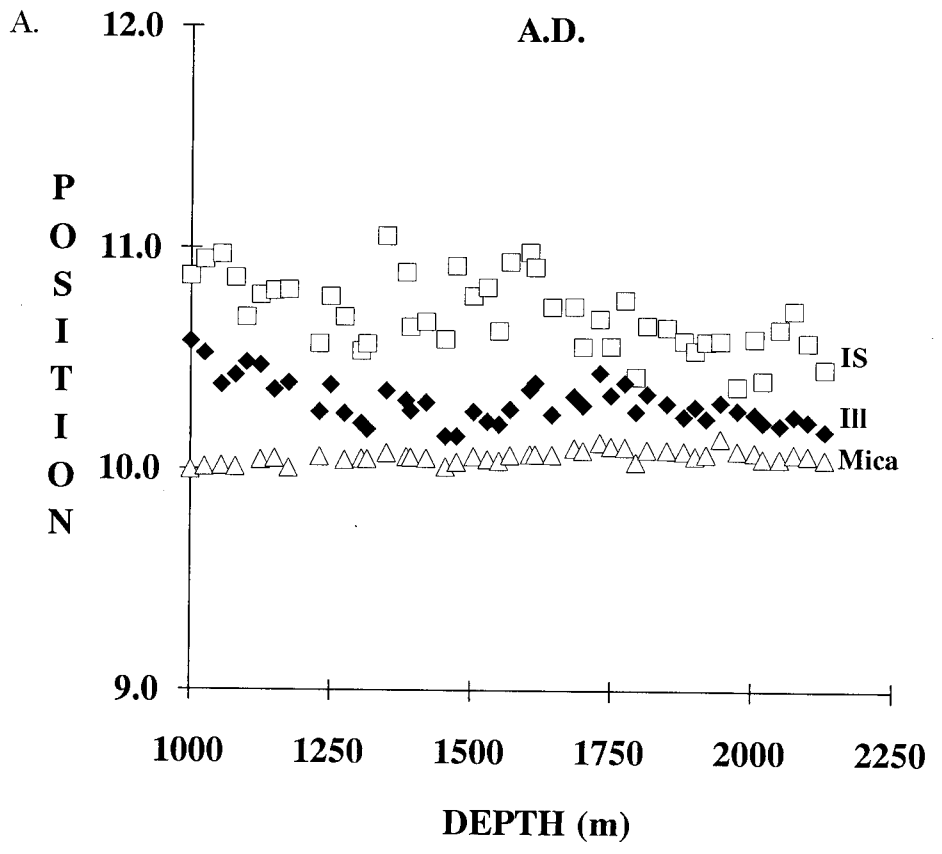

Fig. 8(A) Evolution of elementary peak position (°2θ Cu Kα) with depth for air-dried spectra. The patterns indicate the supposed nature of associated phase (see text): empty triangles: detrital mica; filled diamonds: illite (Ill); empty squares: ordered illite/smectite mixed-layer (IS).

and 4, respectively). The lower value mode can be related to the grain shapes based upon the hexagonal form, whose inscribed ellipse has a theoretical log (L/W) of 0.0, compared to the first maximum on the figure at 0.15. The laths are rather elongate, with a maximum log (L/W) of approx 0.6 which changes little with depth. The maximum is near 1.2 (L/W = 16) suggesting a needle shape. With depth, the lower ratio mode increases while the higher ratio mode becomes less evident.

Using the value at the minimum between the two modes in figure 10A as a division of the two populations, one can analyze the populations of the two grain shapes, hexagon and lath. We consider log (L/W) = 0.48, which corresponds to the aspect ratio of 3.0, as the limit between lath-shaped and hexagonal-shaped particles. Two histograms of grain

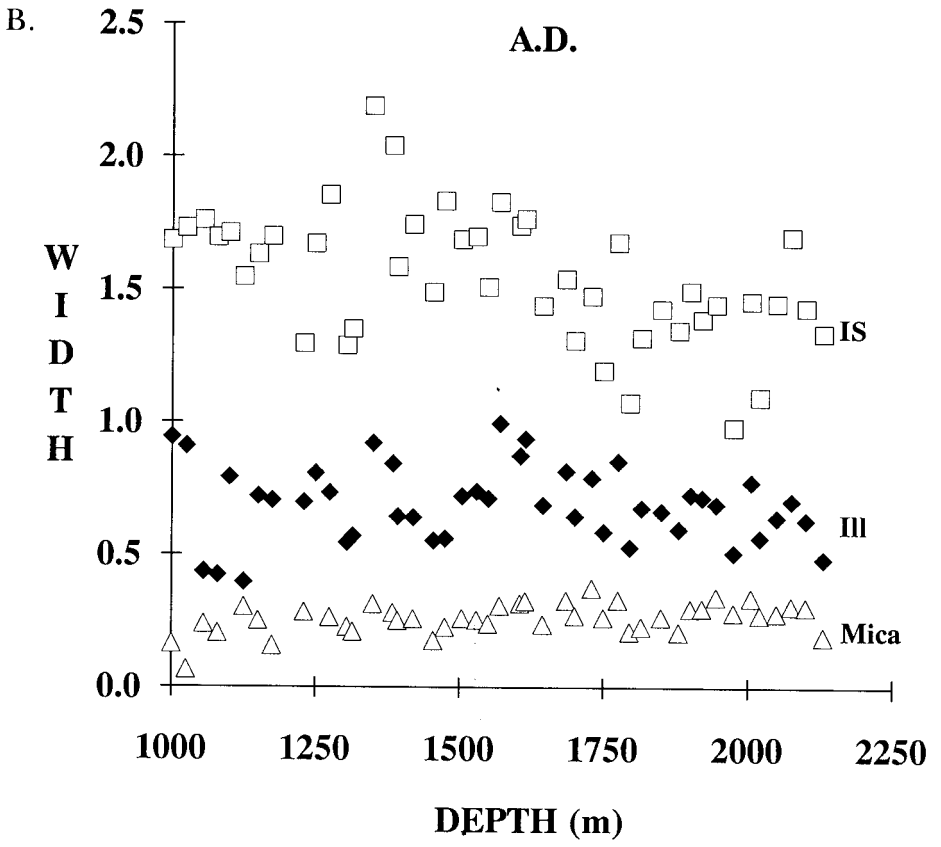

(B) Evolution of elementary peak width (°2θ Cu Kα) with depth for air-dried spectra. Symbols as in (A).

size (equivalent diameter) are established on the basis of aspect ratio, all those with log (L/W) < 0.48 are considered to be derived from a hexagonal shape, and those with log (L/W) > 0.48 are laths. As the two modes overlap to a certain extent, the separation will not be perfect, but it is assumed that the overall trends will be respected in the treatment that follows.

Figure 11 indicates that there is a difference in the distribution of the grain sizes (equivalent diameter) for each shape and in their relative abundance with depth. The laths become relatively less abundant with depth compared to the hexagons. There are no lath-shaped grains in the smallest size fraction measured. Change in relative abundance is taken to indicate a dissolution of the smaller laths in favor of the hexagon-shaped particles. Nevertheless, in the lath population, there are proportionally

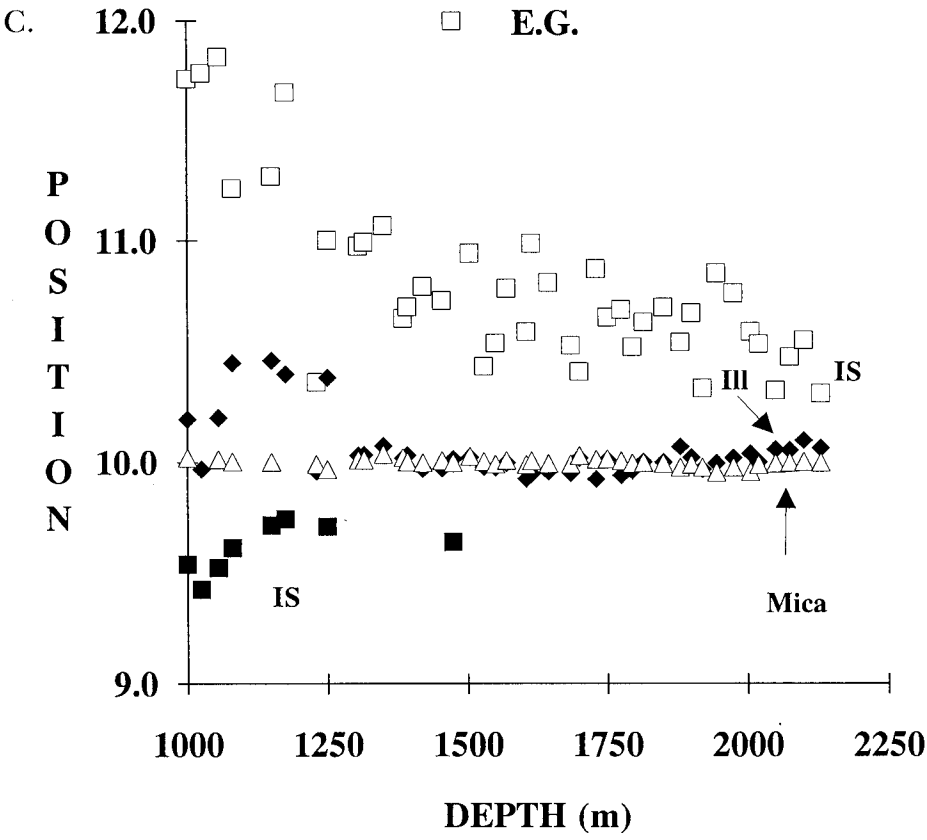

Fig. 8 (continued) (C) Evolution of elementary peak position (°2θ Cu Kα) with depth for glycolated spectra. Symbols as in (A) (solid squares: ordered illite/smectite mixed-layer (IS)).

more large grains with depth. This indicates that the remaining laths continue to grow with depth and age in the sediments.

With increasing depth as the hexagons become relatively more abundant there is a constant proportion of the grains in the smaller sizes. This suggests either a significant phenomenon of germination (creation of small crystallites) or the dissolution of bigger particles. Whichever the case, these phenomenon have to be simultaneous with the hexagons growth, shown by the greater frequency of grains in increasingly larger size fractions.

The above observations on grain abundance and size are taken to indicate that the total population of the lath-shaped grains decreases at the expense of the hexagonal shapes. Both the laths and hexagon-derived shapes continue, on the average, to growth with depth. This results in a change in the shape of the histograms, with an asymmetric

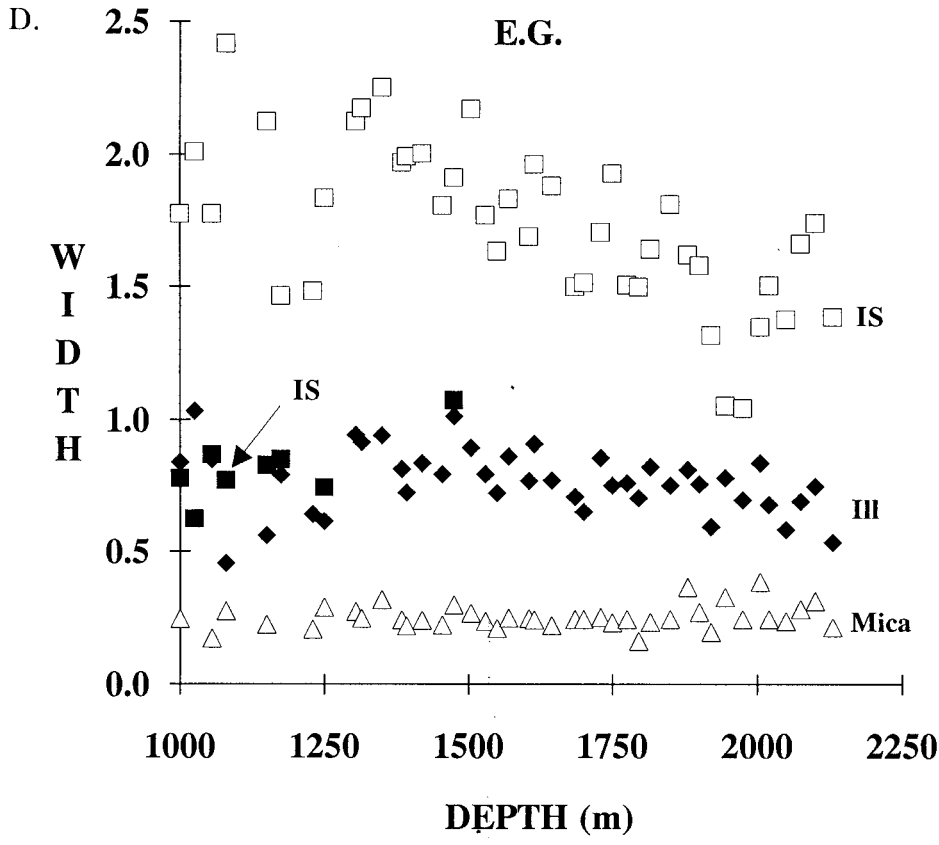

(D) Evolution of elementary peak position (°2θ Cu Kα) with depth for air-dried spectra. Symbols as in (C).

spread to the larger grains sizes, especially marked in the hexagonal type shaped grains. This asymmetry is typical of Ostwald ripening growth sequences (Baronnet, 1982).

In any case, the evolution is toward a lath-free assemblage with depth where the smaller laths disappear first from the assemblage, being replaced by small hexagon shaped particles, while existing hexagons continue to grow.

Microanalysis (XRF).—Particles with characteristic grain shapes were analyzed by X-ray fluorescence (XRF) methods in two of the samples, 1000 m and 2130 m using the electron microscope. As many of the particles were small and very thin, counting times were on the order of 200 sec. Beam diameter was large, near 0.5 μm.

The results were calculated into a mineral formula assuming $O_{10}(OH)_2$ cationic charges. Fe is calculated as Fe^{3+} in all cases and incorporated into

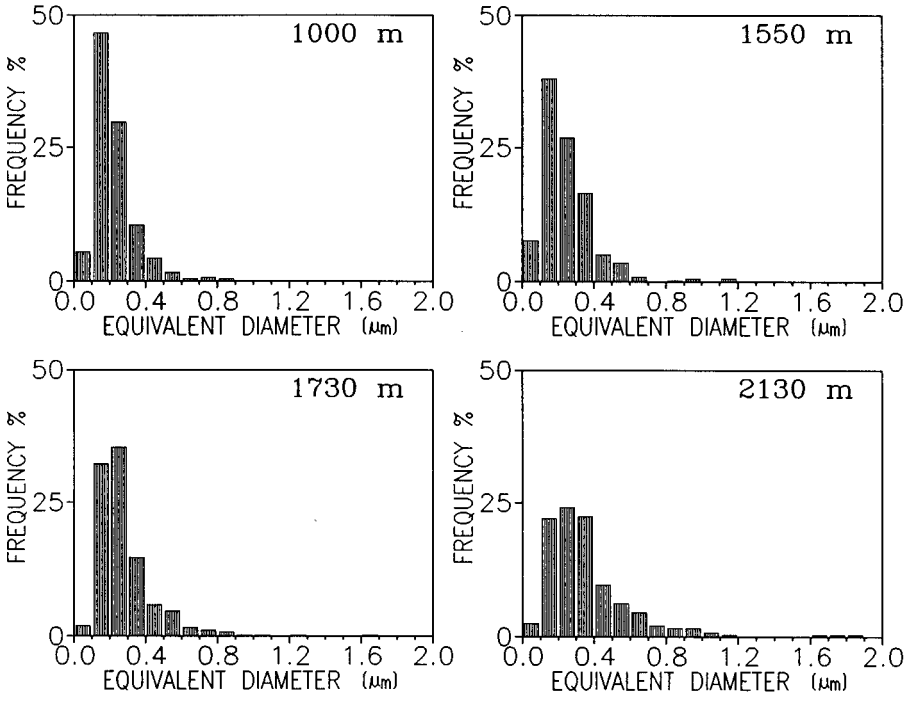

Fig. 9. Histograms of the equivalent diameters (grain sizes for circular particles) in the four samples investigated. Note that the average size changes little with depth.

the octahedrally coordinated ion site. This attribution is probably reasonable in that the rocks contain obvious hematite grains which would tend to buffer the iron in the micas to a ferric state. Results are given in table 1 as averages with standard deviations. All points measured can be found in figure 12A and B where the analyses are plotted in celadonite–muscovite–pyrophyllite coordinates (Yoder and Eugster, 1955). The pyrophyllite component is determined as the value of 1 less the charge on the structure, pyrophyllite will be 100 percent when the charge on the structure is zero. Muscovite content is calculated as 4 less Si content and celadonite is calculated as 2 less the R^{3+} content, Al, and Fe^{3+}. It should be noted that the alkali content (K^+) of the grains is not taken directly into account in the attribution of the molecular components of the diagram. This insures that the effect of possible alkali loss under the electron beam has a minimum effect when comparing the analyses with one another. The alkali content figures only in the calculations of the ionic totals and thus does not greatly affect the calculated formulae.

In each group of particle analyses there is a certain dispersion (fig. 12). This can be due to inherent compositional variation or to experimental error. The magnitude of this latter value is estimated from the analysis

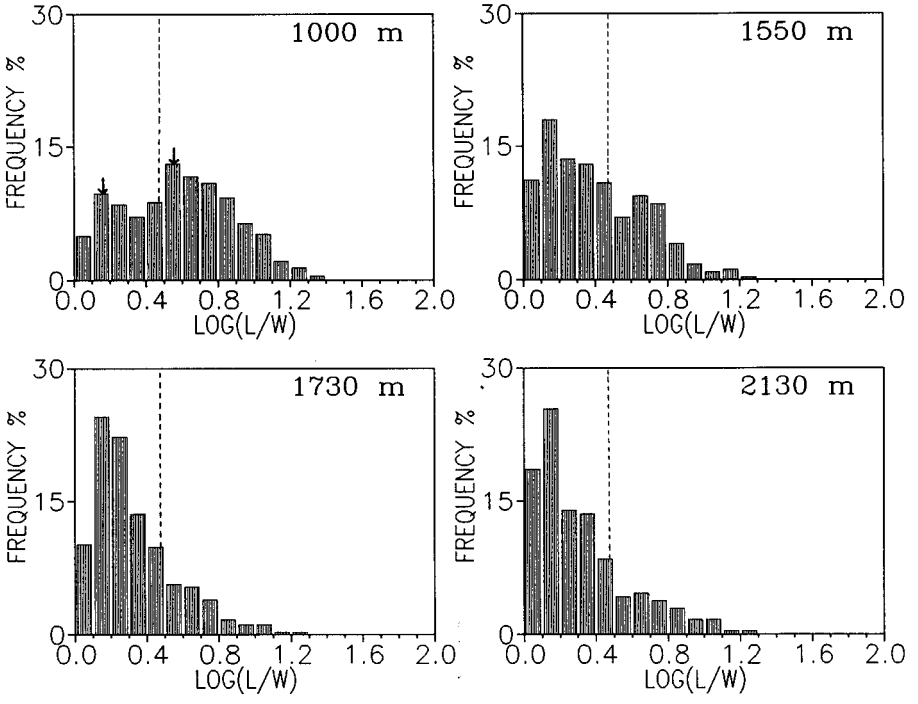

Fig. 10. Frequency versus the log of the length/width (aspect) ratio for the grain in the four samples investigated. In the 1000 m depth well, there is a clear separation at the ratio of 3 (log (3) = 0.48) which is used to distinguish the lath from the hexagonal type grains.

procedure and shown in figure 12. Both the tables and the figures indicate that the analyses of the particles measured show distinct groupings of composition for the laths and hexagons in the two samples analyzed. The compositions of the particles with a hexagonal shape type seem to be roughly the same in the two samples, but the laths seem to be more micaceous (that is, nearer the celadonite-muscovite line) in the deeper sample. The tendency in the laths is to increase both the overall charge and hence potassium content as well as the muscovite component. The trend of compositions is between the mica endmember join and the celadonite-pyrophyllite side of the plot. This indicates that there is a substitution of montmorillonite type molecule as total charge on the structure decreases. This trend has been noted in analyses of aggregate samples, that is, several hundred milligram samples, discussed by Velde and Brusewitz (1986).

INTERPRETATION

Nature and evolution of the particles.—Both XRD decomposition results and TEM/XRF observations reported above indicate the existence of

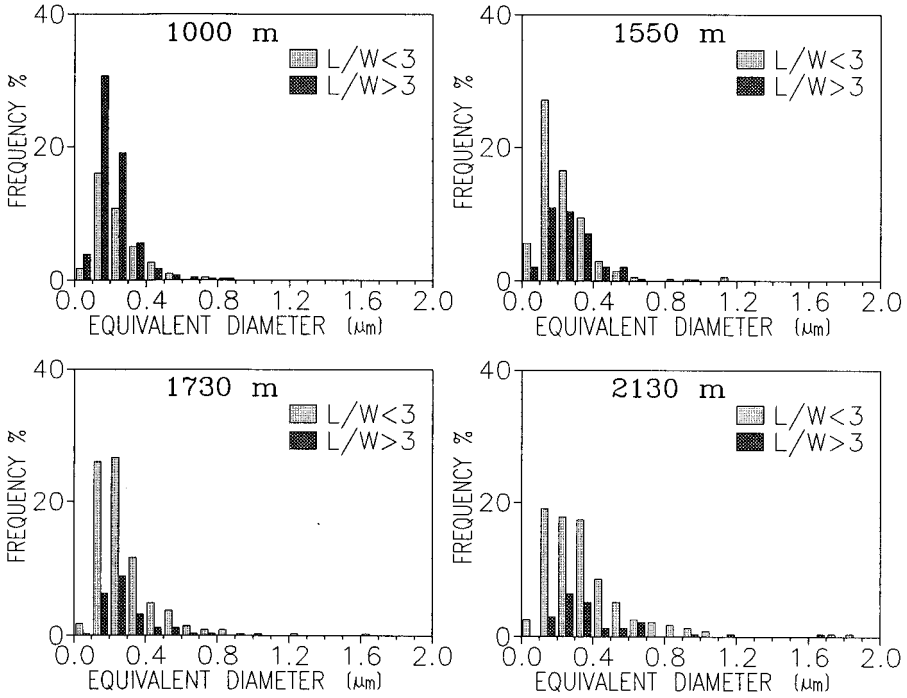

Fig. 11. Distributions of the two different shaped particles as a function of depth. The laths are initially more abundant and replaced by hexagons. The lath grains, although reduced in population, continue to grow in equivalent diameter (surface area). The hexagons become more abundant in the small grain sizes as depth increases, and many grow to larger sizes.

TABLE 1

Mean structural formulae (per $O_{10}(OH)_2$) and standard deviations calculated from atomic concentrations measured on lath-shaped or hexagonal-shaped particles from 1000 and 2130 m deep samples

	Si IV	Al IV	Al VI	Fe VI	Mg VI	O.C.	K Int.	Mg Int.	Charge
Laths 1000 m	3.59	0.41	1.55	0.15	0.30	2.00	0.68	0.01	−0.71
Std. deviation	0.07	0.07	0.08	0.08	0.07	0.02	0.08	0.02	0.05
Hex. Pl. 1000m	3.25	0.75	1.73	0.09	0.19	2.01	0.87	0.01	−0.90
Std. deviation	0.16	0.16	0.14	0.07	0.08	0.01	0.05	0.01	0.07
Laths 2130m	3.40	0.60	1.67	0.15	0.17	1.99	0.79	0.01	−0.81
Std. deviation	0.17	0.17	0.12	0.10	0.09	0.03	0.06	0.02	0.06
Hex. Pl. 2130m	3.25	0.75	1.72	0.12	0.16	2.00	0.91	0.00	−0.92
Std. deviation	0.08	0.08	0.06	0.02	0.05	0.02	0.04	0.01	0.03

IV: Tetrahedral occupancy
VI: Octahedral occupancy
O.C.: number of octahedral cations
Int.: Interfoliar occupancy
Charge: Layer charge
Laths 1000 m: 13 measurements
Laths 2130 m: 14 measurements
Hexagonal plates 1000 m: 5 measurements
Hexagonal plates 2130 m: 18 measurements

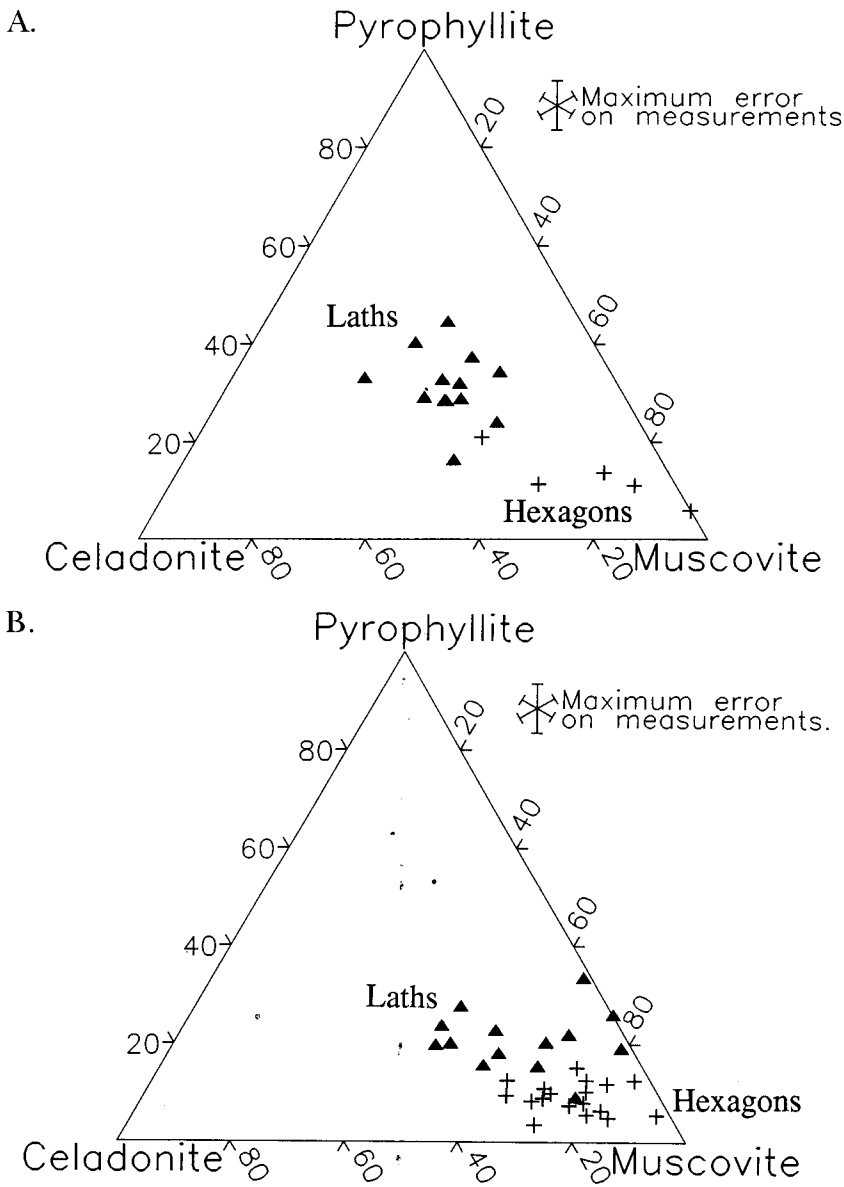

Fig. 12. XRF TEM analyses of the two different shaped grains for 1000 m (A) and 2130 m depth (B) represented in the coordinates of pyrophyllite–celadonite–muscovite. Calculations of the pole contents are given in the text and detailed results in table 1. Triangles represent analyses of the lath shaped particles, and crosses the hexagonal forms. The deeper sample shows an increase of the mica component while the hexagons retain a similar compositional distribution.

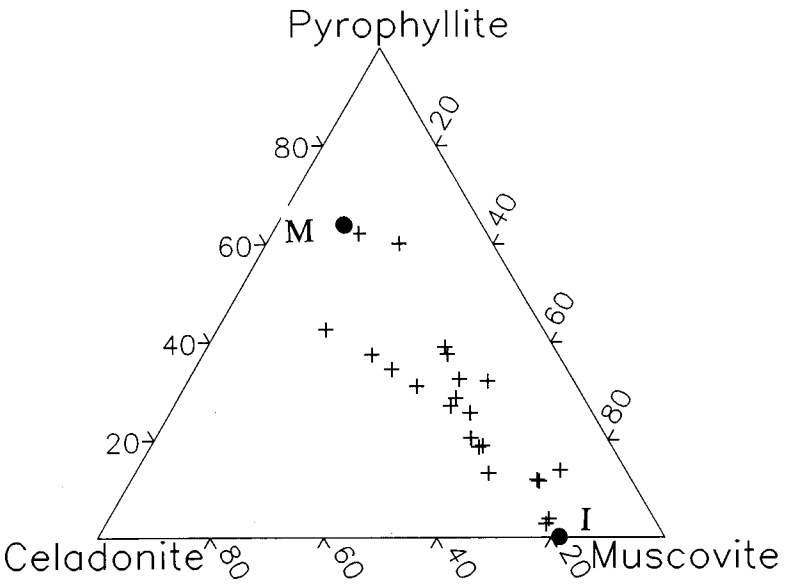

Fig. 13. Plot of grain analyses given by Inoue and others (1987) in the pyrophyllite-celadonite-muscovite coordinates showing a similar series of compositions for hydrothermal vein deposits compared to the diagenetic minerals studied here.

two particles populations: an illitic one which changes little with depth, and an I/S phase which becomes less smectitic with depth. Because of these analogies we assume that the wider, lower angle, elementary XRD peak is associated with lath-shaped I/S particles. The elementary XRD peak with intermediate width and position is related with hexagonal illitic particles. These two types of particles can be characterized as follows:

1. Hexagonal shaped particles have roughly the same composition in the two samples. The charge in both is near 0.9 being derived essentially from substitutions in the tetrahedral site. These particles become dominant in the deeper sample and appear to have become much larger on average at 2130 m than at 1000 m. If one is correct in attributing to these particles the peak with intermediate width and position in the decomposed X-ray diffractograms, the percent expandable layers in the crystallites is very low (< 5 percent Sm). These particles can be called illite.

2. The lath-shaped particles have a charge between 0.7 and 0.8 depending upon the depth, but they show a rather large scatter in their composition in each sample. One can identify them as grains producing the higher spacing diffraction peak in XRD determinations.

The average composition of these lath-shaped particles is found to lie in a trend between that of the hexagonal particles (charge of near 0.9) and montmorillonite with a charge of about 0.4 per layer. In using the average position of the particle's composition on a line between mica-

ceous 0.9 charge illite and montmorillonite, one can estimate the average smectite content of those grains analyzed as being near 40 percent in the 1000 m depth sample and 20 percent in the 2130 m depth sample. These values will probably not be the same as the values determined by X-ray diffraction due to the effect of particle size which accentuates the importance of the larger, thicker particles in the diffractogram due to their greater mass. Indeed, the relative diffraction intensities are not related to the relative frequencies of the different particle sizes but to their relative masses.

3. Simultaneous variation in the alumina content, structural charge, and potassium content of the individual grains demonstrates that each lath-shaped grain contains some layers of a montmorillonite-smectite composition.

These XRD, XRF, and image analysis observations indicate that the populations of the two types of clay particles which coexist in both samples evolve with depth (increase in the parameters of time and temperature). The small laths disappear, all laths become less abundant, and one finds relatively more of smaller as well as larger hexagonal particles. At greatest observed depth the small hexagonal particles become less abundant as the bulk of the particles grow and the average shifts to larger sizes. The remaining laths continue to grow also.

The process of particle size change, that is, skewing to larger grain sizes, is reminiscent of that ascribed to dynamic crystal growth according to the Ostwald ripening process (Baronnet, 1974, 1982). However it is not possible to tell whether the system is closed and the total mass of the material used to nourish the growing phases is constant, as is necessary for a rigorous application of Ostwald ripening. If a significant portion of the growth material comes from the small amount of kaolinite, the feldspars, and detrital micas present in the rocks, the distribution of grain sizes will be due to some sort of growth kinetics which cannot be determined with the data available.

More important, Ostwald ripening can only be used to describe monomineralic systems. We find here a lath-shaped I/S phase and an hexagonal illitic phase, both changing in size and abundance. Such a system cannot be described by Ostwald ripening. However, using the reduced coordinates for the grain size distribution (Baronnet, 1982), we obtain a log-normal distribution (fig. 14A). With the equation

$$f(\omega) = \frac{1}{\omega.\beta.(2.\pi)^{1/2}} \cdot \exp\left(-\frac{1}{2.\beta^2} \cdot (\ln(\omega) - \alpha)^2\right)$$

where

$$\alpha = \Sigma \ln(\omega).f(\omega)$$

and

$$\beta^2 = \Sigma (\ln(\omega) - \alpha)^2.f(\omega)$$

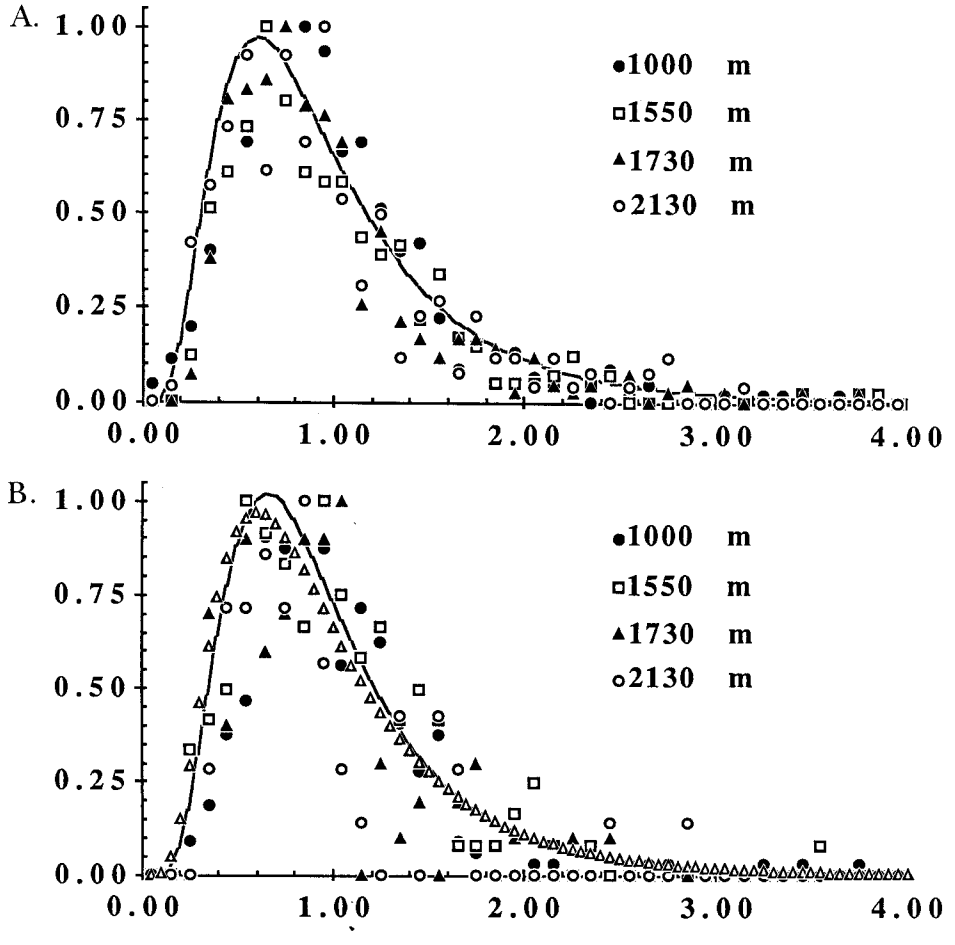

Fig. 14. Particle size distributions plotted on reduced coordinates. (A) Whole samples. The solid line is the log-normal distribution calculated after Eberl and others (1990). (B) Lath-shaped particles. Solid line as above, empty triangles: log-normal distribution calculated for the whole samples.

given by Eberl and others (1990), we can determine the α and β^2 values for this distribution ($\alpha = -0.1707$ and $\beta^2 = 0.3307$). In figure 14A, laths and hexagonal plates were not distinguished. Plotting separately these two kinds of particles (fig. 14B and C, respectively for the laths and the hexagons), one can observe a much greater scatter of the data. In spite of this scatter, the log-normal distributions calculated separately for these two types of particles ($\alpha = -0.1472$, $\beta^2 = 0.2695$ and $\alpha = -0.1848$, $\beta^2 = 0.3668$, respectively for the laths and the hexagons) are close to the

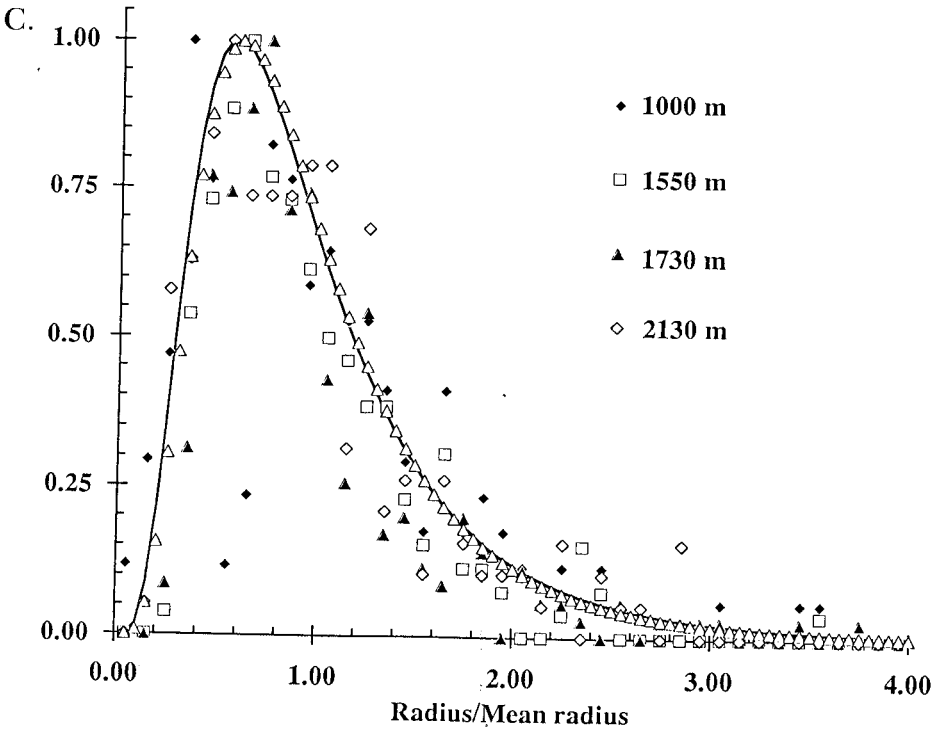

(C) Hexagonal particles. Solid line and empty triangles as above.

values calculated for the whole samples. These analogies suggest that even if Ostwald ripening cannot be applied directly, the driving force of grain growth can be related to the minimization of surface free energy.

The mean grain compositions of the laths vary in a roughly linear fashion between a montmorillonitic smectite composition and an illite composition. The illite composition is assumed to be that of the hexagons, with a 0.9 charge and a small phengitic substitution. This trend, characterized by simultaneous changes in the Si/Al ratio and in the location of the substitutions, strongly suggests that the laths (assumed I/S phases) actually contain smectitic layers. If only the potassium-deficient surface layer gives the expandability observed in the X-ray diffraction diagrams, as the fundamental particle theory suggests (Nadeau and others, 1984a and b), the I/S lath compositions would form a continuous series between a mica composition (celadonite-muscovite edge of fig. 12) and the pyrophyllite pole of the diagram. Instead, we observe that the lath compositions show a continuous compositional change between a point on the celadonite-muscovite mica side and the celadonite-pyrophyllite side of the diagram. This indicates a change in the Si/Al ratio of the phases,

symptomatic of the montmorillonite (smectite) substitution. The laths then contain smaller quantities of smectite as they become larger in size, with depth.

The roughly linear evolution of lath-shaped particles between a montmorillonitic composition and an illitic composition with depth suggests that the material added to both types of crystallites is essentially illitic; this means that it has the same composition as the hexagons, with a charge of near 0.9 and only minor celadonite substitution.

Particles of both shapes grow by precipitation of the same illite material from the same aqueous solution. This does not mean that the whole particles are in thermodynamic equilibrium but is reminiscent of the processes described by Steefel and Van Cappellen (1990) resulting from the presence of different grain sizes and from consequent surface micro-environments. From the eventual predominance of the hexagonal shapes at the expense of the smallest category of laths we can deduce that the factors of time and temperature favor the hexagonal, illite particles. The laths can be considered to be unstable in the context of the burial diagenesis they have undergone. This instability is shown by the dissolution of the smallest particles in the mineral category which feed the growing hexagons. The stability of the bigger laths is related to their low surface free energy.

Comparison with other studies.—TEM and SEM analyses of clay particles in the I/S series have been made previously (Pollastro, 1985; Keller, Reynolds, and Inoue, 1986; Inoue and others, 1988). The lath and hexagon shapes have been recognized in hydrothermal deposition and alteration (Inoue and others, 1988). XRF particle analyses of such material (Inoue and others, 1987) show a slightly different trend from those in the present study of diagenetic material with the smectite component being slightly more beidellitic (fig. 13). The X-ray diffraction analysis estimations of the smectite content by Inoue correlate well with the composition found on the chemical plot of pyrophyllite-celadonite-muscovite content (correlation coefficient of $r = 0.96$ with a deviation of 7.25 percent). The XRD data of Inoue indicate a greater number (N) of coherent layers in the diffracting particles than those of the present study. It is suggested that the closer correspondence between XRD and XRF data of his study is due to thicker particles; simulations are then more realistic.

One can conclude that the diagenetic compositional trend is similar to, but not identical with, other I/S mineral series that form under other geological conditions, notably at higher temperatures and under shorter periods of time (hydrothermal and geothermal areas). All I/S series show concomitant changes of potassium and aluminum content indicating the existence of the low charge, siliceous material in the structure which is montmorillonitic in character. This substantiates the interpretation, already a classical one, that there is a continuous change in smectite content (montmorillonite, in fact) in the smectite-to-illite transition as it nears the illite endmember.

DISCUSSION AND CONCLUSIONS

This study follows essentially the latter part of the I/S transformation, that of the change from an ordered, R = 1 structure I/S to illite. The transformation can be considered as not only a change in smectite (expandable) layer content but also one of dissolution and precipitation. The reaction proposed initially by Hower and others (1976) suggests this fact. Both the decrease in Si, Fe, Mg contents and the increase in Al and K contents, necessary to effect the change from a montmorillonitic smectite to illite, imply dissolution-recrystallization, as suggested by Nadeau and others (1985) and Boles and Franks (1979). Velde and Brusewitz (1986) have analyzed the chemical changes in I/S mineral series from various geological environments and find that the dominant smectite substitution in all is that of montmorillonite where the charge is developed by substitution of an octahedral divalent ion for a trivalent one. As proposed by Boles and Franks (1979) among many others, the released elements can be transferred to a neoformed chlorite through their reaction with kaolinite or, as observed in hydrothermal experiments on natural clays, the chlorite component is exolved from the I/S minerals (Velde, 1977).

Thus the conversion of I/S or smectite to illite will depend upon elements in solution, reacting solids other than I/S minerals, and the relative abundance of solution to solids in the reacting zone. The openness of pore space, and the composition of the solutions, will determine whether the diagenetic system will be one of chemical migration (an open system) or one of essentially constant composition (closed system). The nature and the proportion of reacting phases will probably not be the same in the two cases.

Despite the potential complexity of the reaction of smectite to form illite, the change in morphology of the I/S minerals near the illite composition reflects a change in mineral stability. The I/S becomes unstable, and the illite, mica-like phase is the stable aluminous clay. This change is a gradual one, as has been observed by many authors in studies of burial diagenesis. This coexistence or co-presence of two types of illitic shapes has been noted in Gulf Coast by many authors using XRD methods. Such a situation is to be expected in a system at low temperatures, where phase changes will be slow and the zone of bi-phase mineralogy representing mineral transition will be extended in time-temperature space.

The most important conclusion to be drawn from the present study is that the lath-like I/S mineral particles grow (change illitic content) and become unstable with respect to hexagonal, micaceous illite. This means that the smectite-to-illite transition is not one continuous reaction but is accomplished by several reactions, with apparently the same growth process, driven by the minimization of surface free energy.

ACKNOWLEDGMENTS

We greatly thank B. Velde for his constant encouragements and for many helpful discussions during this work. The authors would like to

thank the Institut Français du Pétrole for supplying the samples used in the study. The precious help of G. Besson, Université of Orléans, A. Meunier, Université of Poitiers, and Jan Srodon, Polish Academy, are gratefully acknowledged, as well as constructive reviews by D. D. Eberl and P. A. Schroeder. Financial support (B.L.) was provided by the Institut Français du Pétrole.

REFERENCES

Ahn, J. H., and Peacor, D. R. 1986, Transmission and analytical electron microscopy of the smectite-to-illite transition: Clays and Clay Minerals, v. 34, p. 165–179.

———— 1989, Illite/smectite from Gulf Coast shales: a reappraisal of transmission electron microscope images: Clays and Clay Minerals, v. 37,p. 542–546.

Baronnet, A., 1974, Etude en microscopie électonique des premiers stades de croissance d'un mica synthétique, la phlogopite hydroxylée. Phénomènes de coalescence et mûrissement dans le système fermé conservatif: K_2O-6MgO-Al_2O_3-6SiO_2-excès H_2O: High Temperatures-High Pressures, v. 6, p. 675–685.

———— 1982, Ostwald ripening in solution. The case of calcite and micas: Estudios Geologicos, v. 38, p. 185–198.

Boles, J. R., and Franks, S. G., 1979, Clay diagenesis in Wilcox sandstones of southwest Texas: implications of smectite diagenesis on sandstone cementation: Journal of Sedimentary Petrology, v. 49, p. 55–70.

Burst, J. F., 1969, Diagenesis of Gulf Coast clayey sediments and its possible relation to petroleum migration: American Association of Petroleum Geologists Bulletin, v. 53, p. 73–93.

Champion, D., ms, 1989, Etude des mécanismes de transformation des interstratifiés illite/smectite au cours de la diagenèse: Ph.D. thesis, University Orsay, France, 204 p.

Cliff, G., and Lorimer, G. W., 1975. The quantitative analysis of speciments: Journal of Microscopy, v. 103, p. 203–207.

Eberl, D. D., and Srodon, J., 1988, Ostwald ripening and interparticle-diffraction effects for illite crystals: American Mineralogist, v. 73, p. 1335–1345.

Eberl, D. D., Srodon, J., Kralik, M., Taylor, B. E., and Peterman, Z. E., 1990, Ostwald ripening of clays and metamorphic minerals: Science, v. 248, p. 474–477.

Freed, R. L., and Peacor, D. R., 1989, Variability in temperature of the smectite/illite reaction in Gulf Coast sediments: Clay Minerals, v. 24, p. 171–180.

Glasmann, J. R., Larter, S., Briedis, N. A., and Lundegard, P. D., 1989, Shale diagenesis in the Bergen High area, North Sea: Clays and Clay Minerals, v. 37, p. 97–112.

Guthrie, G. D., and Veblen, D. R., 1989, High-resolution transmission electron microscopy of mixed-layer illite/smectite: computer simulations: Clays and Clay Minerals, v. 37, p. 1–11.

Güven, N., Hower, W. F., and Davies, D. K., 1980, Nature of authigenic illites in sandstone reservoirs: Journal of Sedimentary Petrology, v. 50, p. 761–766.

Horton, D. G., 1985, Mixed-layer illite/smectite as a paleotemperature indicator in the amethyst vein system, Creede district, Colorado, USA: Contributions to Mineralogy and Petrology, v. 91, p. 171–179.

Hower, J., Eslinger, E. V., Hower, M., and Perry E. A., 1976, Mechanism of burial metamorphism of argillaceous sediments: I Mineralogical and chemical evidence: Geological Society of America Bulletin, v. 87, p. 725–737.

Inoue, A., 1986, Morphological change in a continuous smectite-to-illite conversion series by scanning and transmission electron microscopies: Journal of the College of Arts and Sciences, Chiba University, Japan, B-19, p. 23–33.

Inoue, A., Kohyama, N., Kitagawa, R., and Watanabe, T., 1987, Chemical and morphological evidence for the conversion of smectite to illite: Clays and Clay Minerals, v. 35, p. 111–120.

Inoue, A., and Utada, M., 1983, Further investigations of a conversion series of dioctahedral mica/smectites in the Shinzan hydrothermal alteration area, northeast Japan: Clays and Clay Minerals, v. 31, p. 401–412.

Inoue, A., Velde, B., Meunier, A., and Touchard, G., 1988, Mechanism of illite formation during smectite-to-illite conversion series by scanning and transmission electron microscopes: American Mineralogist, v. 73, p. 1325–1334.

Jennings, S., and Thompson, G. R., 1986, Diagenesis of Plio-Pleistocene sediments of the Colorado river delta, southern California: Journal of Sedimentary Petrology, v. 56, p. 89–98.

Keller, W. D., Reynolds, R. C., and Inoue, A., 1986, Morphology of clay minerals in the smectite-to-illite conversion series by scanning electron microscopy: Clays and Clay Minerals, v. 34, p. 187–197.

Lahann, R. W., 1980, Smectite diagenesis and sandstone cement: the effect of reaction temperature: Journal of Sedimentary Petrology, v. 50, p. 755–760.

Lanson, B., ms, 1990, Mise en évidence des mécanismes réactionnels des interstratifiés illite/smectite au cours de la diagenèse: Ph.D. thesis, University Paris 6, France, 366 p.

Lee, J. H., Ahn, J. H., and Peacor, D. R., 1985, Textures in layered silicates: Progressive changes through diagenesis and low-temperature metamorphism: Journal of Sedimentary Petrology, v. 55, p. 532–540.

Mac Dowell, S. D., and Elders, W. A., 1980, Authigenic layer silicate minerals in borehole Elmore 1, Salton Sea geothermal field, California, USA: Contributions to Mineralogy & Petrology, v. 74, p. 293–310.

Meunier, A., and Velde, B., 1989, Solid solutions in illite/smectite mixed layer minerals and illite: American Mineralogist, v. 74, p. 1106–1112.

Nadeau, P. H., and Reynolds, R. C. Jr, 1981, Burial and contact metamorphism in the Mancos Shale: Clays and Clay Minerals, v. 29, p. 249–259.

Nadeau, P. H., Tait, W. J., McHardy, W. J., and Wilson, M. J., 1984a, Interstratified XRD characteristics of physical mixtures of elementary clay particles: Clay Minerals, v. 19, p. 67–76.

Nadeau, P. H., Wilson, M. J., McHardy, W. J., and Tait, J. M., 1984b, The conversion of smectite to illite during diagenesis: evidence from illite clays from bentonites and sandstones: Mineralogical Magazine, v. 49, p. 393–400.

———— 1985, The conversion of smectite to illite during diagenesis: evidence from some illitic clays from bentonites and sandstones: Mineralogical Magazine, v. 49, p. 393–400.

Nelder, J. A., and Mead, R., 1965: Computer Journal, v. 7, p. 308.

Perry, E. A., Jr., and Hower, J., 1970, Burial diagenesis in Gulf Coast pelitic sediments: Clays and Clay Minerals, v. 18, p. 165–177.

Pollastro, R. M., 1985, Mineralogical and morphological evidence for the formation of illitic at the expense of illite/smectite: Clays and Clay Minerals, v. 33, p. 265–274.

Reynolds, R. C., 1980, Interstratified clay minerals, *in* Brindley, G. W., and Brown, G., editors, Crystal Structures of Clay Minerals and Their X-ray Identification: Mineralogical Society, London, p. 249–359.

———— 1985, NEWMOD© a computer program for the calculation of one-dimensional patterns of mixed-layered clays: Hanover, New Hampshire 03755, R. C. Reynolds, 8 Brook Rd.

———— 1986, The Lorentz-polarization factor and preferred orientation in oriented clay aggregates: Clays and Clay Minerals, v. 34, p. 359–367.

———— 1989, Diffraction by small and disordered crystals, *in* Bish, D. L., and Post, J. E., editors, Modern Powder Diffraction: Mineralogical Society of America, Reviews in Mineralogy, v. 20, p. 145–181.

Reynolds, R. C., and Hower, J., 1970, The nature of interlayering in mixed-layer illite-montmorillonites: Clays and Clay Minerals, v. 18, p. 25–36.

Srodon, J., 1979, Correlation between coal and clay diagenesis in the Carboniferous of the upper Silesian coal basin, *in* Mortland, M. M., and Farmer, V. C., editors, Proceedings of International Clay Conference, Oxford 1978: Amsterdam, Elsevier, p. 251–260.

———— 1980, Precise identification of illite/smectite interstratifications by X-ray powder diffraction: Clays and Clay Minerals, v. 28, p. 401–411.

———— 1984a, Mixed-layer illite-smectite in low-temperature diageneis: data from the Miocene of the Carpathian foredeep: Clay Minerals, v. 19, p. 205–215.

———— 1984b, X-ray powder diffraction of illitic materials: Clays and Clay Minerals, v. 32, p. 337–349.

Srodon, J., and Eberl, D. D., 1984, Illite, *in* Bailey S. W., editor, Micas: Mineralogical Society of America, Reviews in Mineralogy, v. 13, p. 495–544.

Steefel, C. I., and Van Cappellen, P., 1990, A new kinetic approach to modeling water-rock interaction: The role of nucleation, precursors, and Ostwald ripening: Geochimica et Cosmochimica Acta, v. 54, p. 2657–2677.

Van der Pluijm, B. A., Lee, J. H., and Peacor, D. R., 1988, Analytical electron microscopy and the problem of potassium diffusion: Clays and Clay Minerals, v. 36, p. 498–504.

Velde, B., 1977, A proposed phase diagram for illite, expanding chlorite, corrensite and illite-montmorillonite mixed layered minerals: Clays and Clay Minerals, v. 25, p. 264–270.

———— 1985, Clay Minerals: A Physico-chemical Explanation of their Occurrence: Amsterdam, Elsevier, p. 427.

Velde, B., and Brusewitz, A. M., 1982, Metasomatic and non-metasomatic low grade metamorphism of Ordovician meta-bentonites in Sweden: Geochimica et Cosmochima Acta, v. 46, p. 447–452.

———— 1986, Compositional variation in component layers in natural illite/smectite: Clays and Clay Minerals, v. 34, p. 651–657.

Velde, B., and Espitalié, J., 1989, Comparison of kerogen maturation and illite/smectite composition in diagenesis: Journal of Petroleum Geology, v. 12, p. 103–110.

Velde, B., Suzuki, T., and Nicot, E., 1986, Pressure-Temperature-Composition of illite/smectite mixed-layer minerals: Niger delta mudstones and other examples: Clays and Clay Minerals, v. 34, p. 435–441.

Warren, B. E., and Averbach, B. L., 1950, The effect of cold-work distortion on X-ray patterns, Journal of Applied Physics, v. 21, p. 595–599.

Watanabe T., 1988, The structural model of illite/smectite interstratified mineral and the diagram for their identification: Clay Science, v. 7, p. 97–114.

Yoder, H. S., and Eugster, H. P., 1955, Synthetic and natural muscovites: Geochimca et Cosmochima Acta, v. 8, p. 225–280.